# Estimation of Illuminant Direction, Albedo, and Shape from Shading*

Qinfen Zheng and Rama Chellappa

Signal and Image Processing Institute
Department of Electrical Engineering Systems
University of Southern California
Los Angeles, CA 90089-0272

## Abstract

A robust approach to recovery of shape from shading information is presented. Assuming uniform albedo and Lambertian surface for the imaging model, we first present methods for the estimation of illuminant direction and surface albedo. The illuminant azimuth is estimated by averaging local estimates. The illuminant elevation and surface albedo are estimated from image statistics. Using the estimated reflectance map parameters, we then compute the surface shape using a new procedure, which implements the smoothness constraint by enforcing the gradients of reconstructed intensity to be close to the gradients of the input image. Typical results on real images are given to illustrate the usefulness of our approach.

## 1 Introduction

Shape from shading (SFS)[1] refers to the process of reconstructing the 3-D shape of an object from its 2-D intensity image. In computer vision, SFS is implemented by first modeling the image brightness as a function of surface geometry and then reconstructing a surface which, under the given imaging model, generates an image close to the input image.

In this paper, we use the most commonly used Lambertian imaging model [2]:

$$\mathcal{R}(p,q) = \eta \frac{\cos\gamma - p\cos\tau\sin\gamma - q\sin\tau\sin\gamma}{\sqrt{1+p^2+q^2}} + \sigma_0 \quad (1)$$

where $\eta$ is the composite albedo, that includes factors such as strength of illumination and the reflectivity of the surface. For uniform illumination, $\eta$ is constant if the surface is optically uniform. $\vec{N} = (-p,-q,1)/\sqrt{1+p^2+q^2}$ is the surface normal at position $(x,y,z(x,y))$ [2]. $\vec{L} = (\cos\tau\sin\gamma, \sin\tau\sin\gamma, \cos\gamma)$ is the unit vector for the illuminant direction, where $\tau$ and $\gamma$ are the tilt and slant angles. $\vec{L}$ is constant for parallel illumination. $\sigma_0$ is the bias brightness depending on background illumination, digitizer calibration, etc. Several algorithms [3, 4, 5, 6, 7] are available for estimation of $(\tau,\gamma,\eta)$ of (1). Most of the known illuminant direction estimators do not work well for complicated scenes and/or when the $\gamma$ of the illuminant is not small, due to inappropriate surface models assumed and the effects of self shadow not being accounted for. In this paper, we introduce a new reflectance map parameters estimator. In our method, $\tau$ is estimated by averaging local estimates. $\gamma$ and $\eta$ are solved from image statistics. The issue of self-shadowing is also addressed.

A commonly used SFS approach is to formulate the SFS problem in a constrained optimization framework [7]. A typical cost function is [1, 7, 8, 9]

$$\iint [I(x,y) - \mathcal{R}(p,q)]^2 + \lambda(p_x^2 + p_y^2 + q_x^2 + q_y^2) + \mu[(z_x - p)^2 + (z_y - q)^2]\, dxdy \quad (2)$$

where the second term is the regularization term often used to ensure the convergence of the iteration process. This term pushes the reconstruction towards a smooth surface. Although it helps to stabilize the minimization process, it has several drawbacks [10]. A solution to this problem is to use an adaptive Lagrangian multiplier to reduce oversmoothing along image boundaries [9]. Another solution is to let $\lambda$ gradually decrease as the iterations proceed[7]. In this paper, we introduce a new cost function which does not have the commonly used quadratic regularization term. Instead, we enforce the gradients of the reconstructed image to be close to the gradients of the input image. Using cal-

*Partially supported by the National Science Foundation Under the Grant MIP-84-51010.

culus of variations [11] and a linear approximation of the reflectance map [7], an iterative scheme which simultaneously updates the slope and height maps is developed.

The rest of this paper is organized as follows: Section 2 discusses our reflectance map parameter estimator. Section 3 presents the SFS algorithm. In Section 4 we present experimental results. The work is summarized in Section 5.

# 2 Estimation of Parameters

## 2.1 Image Model

Let the surface normal $\vec{N}$ be represented by

$$\vec{N} = (\cos\alpha \sin\beta, \sin\alpha \sin\beta, \cos\beta) \tag{3}$$

where $\alpha = \alpha(x, y)$ and $\beta = \beta(x, y)$ are the tilt and slant angles of the surface normal at $(x, y, z(x, y))$. After substitution of (3) into (1), the reflectance map can be rewritten as

$$\mathcal{R}(p, q) = \eta(\cos(\alpha - \tau)\sin\beta\sin\gamma + \cos\beta\cos\gamma) + \sigma_0 \tag{4}$$

## 2.2 $\tau$ Estimate

Let us assume that for any point $(x_o, y_o, z(x_o, y_o))$, its neighbors can be locally approximated by a spherical patch:

$$\begin{cases} x = a(x_o, y_o) + r(x_o, y_o)\sin\beta\cos\alpha \\ y = b(x_o, y_o) + r(x_o, y_o)\sin\beta\sin\alpha \\ z = c(x_o, y_o) + r(x_o, y_o)\cos\beta \end{cases} \tag{5}$$

where $(a(x_o, y_o), b(x_o, y_o), c(x_o, y_o))$ is the center of the sphere and $r(x_o, y_o)$ is the radius of the sphere. For a small increment along the direction $\vec{s} = (\delta x, \delta y)$, the corresponding increments in $(\alpha, \beta)$ is $(\delta\alpha_s, \delta\beta_s)$ and the following relations hold

$$\delta x = -r\sin\beta\sin\alpha\,\delta\alpha_s + r\cos\beta\cos\alpha\,\delta\beta_s \tag{6}$$

$$\delta y = r\sin\beta\cos\alpha\,\delta\alpha_s + r\cos\beta\sin\alpha\,\delta\beta_s \tag{7}$$

$$\sin\beta\,\delta\beta_s = \frac{-\sin\beta\cos\alpha\,\delta x - \sin\beta\sin\alpha\,\delta y}{r\cos\beta} \tag{8}$$

Using (6–8), an increment in (4) due to $(\delta\alpha_s, \delta\beta_s)$ is:

$$\delta I_s = \frac{\eta}{r}(\delta x, \delta y)\begin{pmatrix} \sin\gamma\cos\tau - \cos\gamma\tan\beta\cos\alpha \\ \sin\gamma\sin\tau - \cos\gamma\tan\beta\sin\alpha \end{pmatrix}.$$

Let $\vec{s}$ take different directions yielding

$$d\vec{I} = B\vec{X}$$

where

$$d\vec{I} = \begin{pmatrix} \delta I_1 \\ \delta I_2 \\ \vdots \\ \delta I_N \end{pmatrix}, \quad B = \begin{pmatrix} \delta x_1 & \delta y_1 \\ \delta x_2 & \delta y_2 \\ \vdots & \vdots \\ \delta x_N & \delta y_N \end{pmatrix},$$

$$\vec{X} = \begin{pmatrix} \tilde{x}_L \\ \tilde{y}_L \end{pmatrix} = \frac{\eta}{r}\begin{pmatrix} \sin\gamma\cos\tau - \cos\gamma\tan\beta\cos\alpha \\ \sin\gamma\sin\tau - \cos\gamma\tan\beta\sin\alpha \end{pmatrix},$$

$N$ is the number of measured directions for $\vec{s}$, and $\tilde{x}_L$ and $\tilde{y}_L$ are the $x$ and $y$ components of the local estimate. $\vec{X}$ can be solved using

$$\vec{X} = (B^t B)^{-1} B^t d\vec{I}.$$

It can be proved that[10]

$$\mathbf{E}_{x,y}\left\{\frac{\tilde{x}_L}{\sqrt{\tilde{x}_L^2 + \tilde{y}_L^2}}\right\} = \cos\tau \cdot F(\gamma) \tag{9}$$

and

$$\mathbf{E}_{x,y}\left\{\frac{\tilde{y}_L}{\sqrt{\tilde{x}_L^2 + \tilde{y}_L^2}}\right\} = \sin\tau \cdot F(\gamma) \tag{10}$$

where

$$F(\gamma) = \int_{\Omega_\beta} p(\beta)\,d\beta \frac{1}{2\pi}\int_{-\pi}^{\pi} (\sin\gamma\cos\beta - \cos\gamma\sin\beta\cos\alpha) / \sqrt{\sin^2\gamma\cos^2\beta + \cos^2\gamma\sin^2\beta - \frac{1}{2}\sin 2\gamma\sin 2\beta\cos\alpha}\,d\alpha$$

The illuminant azimuth can be estimated as

$$\tau = \arctan\left(\frac{\mathbf{E}_{x,y}\left\{\frac{\tilde{y}_L}{\sqrt{\tilde{x}_L^2+\tilde{y}_L^2}}\right\}}{\mathbf{E}_{x,y}\left\{\frac{\tilde{x}_L}{\sqrt{\tilde{x}_L^2+\tilde{y}_L^2}}\right\}}\right). \tag{11}$$

## 2.3 Estimation of $\gamma$ and $\eta$

For estimating $\gamma$ and $\eta$, we use the statistical properties of $\alpha$ and $\beta$. For a general scene, the range of $\alpha$ could be $[0, 2\pi)$. Since there is no preference for the tilt angle, an acceptable assumption regarding the distribution of $\alpha$ is

$$p_\alpha = \frac{1}{2\pi}.$$

On the other hand, for the distribution of $\beta$, the effects of self occlusion and foreshortening should be considered. In 3-D space, it is equally possible for a surface patch to have a slant angle between 0 and $\pi$; but due to self occlusion only patches facing the camera can be seen, so the range of $\beta$ is $[0, \pi/2]$. After consideration

of projection effect, the distribution of $\beta$ in the image plane is

$$p_\beta = \cos\beta$$

For general images, we can assume that $\alpha$ and $\beta$ are independent. The statistical model for the normal direction of the surface is

$$p_{\alpha\beta} = p_\alpha \cdot p_\beta = \frac{\cos\beta}{2\pi}. \tag{12}$$

With (12) we can consider the statistical moments of image intensity. Special care should be taken in regions where shadow is present. Here we only consider the case of self shadowing. For a pixel, if the incidence angle is greater than $\pi/2$, the pixel will not be illuminated and its brightness is zero. So the actual image intensity is

$$I(\alpha,\beta)=\max\{\eta[\cos(\alpha-\tau)\sin\beta\sin\gamma+\cos\beta\cos\gamma],\,0\}$$

The first two moments of image intensities are

$$\overline{I} = \frac{1}{2\pi}\int_0^{2\pi}\int_0^{\pi/2} I(\alpha,\beta)\cos\beta\,d\alpha\,d\beta$$

$$\overline{I^2} = \frac{1}{2\pi}\int_0^{2\pi}\int_0^{\pi/2} I^2(\alpha,\beta)\cos\beta\,d\alpha\,d\beta$$

The curve

$$\cos(\alpha-\tau)\sin\beta\sin\gamma+\cos\beta\cos\gamma = 0$$

is an ellipse. Due to symmetry we know that $\overline{I}$ and $\overline{I^2}$ are functions of $\gamma$ and $\eta$ only and can be written as:

$$\overline{I} = \eta f_1(\gamma) \qquad \text{and} \qquad \overline{I^2} = \eta^2 f_2(\gamma),$$

where

$$f_1(\gamma) = \frac{1}{2\pi\eta}\int_0^{2\pi}\int_0^{\pi/2} I(\alpha,\beta)\cos\beta\,d\alpha\,d\beta$$

$$f_2(\gamma) = \frac{1}{2\pi\eta^2}\int_0^{2\pi}\int_0^{\pi/2} I^2(\alpha,\beta)\cos\beta\,d\alpha\,d\beta.$$

We compute $f_1(\gamma)$, $f_2(\gamma)$, and $f_3(\gamma) = f_1(\gamma)/\sqrt{f_2(\gamma)}$ by a numerical method and approximate the results by 7th order polynomials of $\cos\gamma$. The results are

$$f_1(\gamma) \approx \sum_{i=0}^{7} a_i\cos^i\gamma$$

$$f_2(\gamma) \approx \sum_{i=0}^{7} b_i\cos^i\gamma$$

$$f_3(\gamma) \approx \sum_{i=0}^{7} c_i\cos^i\gamma$$

where the coefficients are

| $i$ | $a_i$ | $b_i$ | $c_i$ |
|---|---|---|---|
| 0 | 0.1615 | 0.0834 | 0.5577 |
| 1 | 0.3959 | 0.2169 | 0.6240 |
| 2 | 0.3757 | 0.2487 | 0.1882 |
| 3 | -0.0392 | 0.1836 | -0.6514 |
| 4 | -0.3077 | 0.0048 | -0.53450 |
| 5 | 0.1174 | -0.1086 | 0.9282 |
| 6 | 0.1803 | -0.0043 | 0.3476 |
| 7 | -0.0984 | 0.0424 | -0.4984 |

Since $f_3(\gamma)$ is a monotonically decreasing function of $\gamma$, $\gamma$ can be uniquely solved from

$$\frac{\overline{I}}{\sqrt{\overline{I^2}}} = f_3(\gamma)$$

Subsequently, $\eta$ can be computed by

$$\eta=\frac{1}{f_1^2(\gamma)+f_2(\gamma)}\left(\overline{I}\cdot f_1(\gamma)+\sqrt{\overline{I^2}\cdot f_2(\gamma)}\right)$$

In our implementation of this method, we let $\gamma = 0°$ when $\frac{\overline{I}}{\sqrt{\overline{I^2}}} > f_3(0) = 0.96191$.

# 3 Shape from Shading

## 3.1 Formulation

Once the reflectance map parameters are estimated, the possible surface is determined by the image intensity information. Traditionally, the requirement that reconstructed surface be consistent with observed image is enforced by the irradiance equation:

$$\mathcal{R}(p,q) = I(x,y). \tag{13}$$

It seems that (13) has used all the information contained in the input image, but in iterative SFS algorithms, $p$ and $q$ are updated separately at each pixel. No relationship among the neighboring pixels is enforced. So the quadratic smoothness term is used in (2) to enforce the reconstructed surface to be smoothly connected. Unfortunately, the quadratic smoothness term uniformly suppresses changes in surface shape, irrespective of changes in intensities. In areas, where image intensity changes rapidly, the corresponding surface part may not be smooth, and smoothing over this region should be reduced. This adaptive smoothing idea can be implemented efficiently by requiring the gradients of the reconstructed intensity to be equal to the gradients of the input image. By incorporating these constraints, computation of shape from shading can be formulated as an optimization problem minimizing

$$\iint F(p,q,Z)\,dxdy \tag{14}$$

where

$$\begin{aligned} F &= [\mathcal{R}(p,q) - I(x,y)]^2 + \\ &\quad [\mathcal{R}_p(p,q)p_x + \mathcal{R}_q(p,q)q_x - I_x(x,y)]^2 + \\ &\quad [\mathcal{R}_p(p,q)p_y + \mathcal{R}_q(p,q)q_y - I_y(x,y)]^2 + \\ &\quad \mu[(p - Z_x)^2 + (q - Z_y)^2] \end{aligned} \tag{15}$$

The last term in (15) comes from the integrability constraint [11, 12], where $\mu$ is a weighting factor. Note that the commonly used quadratic smoothness term present in almost all published works has been dropped. Using calculus of variations, minimization of (14) is equivalent to solving the following Euler equations:

$$\begin{cases} F_p - \frac{\partial}{\partial x}F_{p_x} - \frac{\partial}{\partial y}F_{p_y} &= 0 \\ F_q - \frac{\partial}{\partial x}F_{q_x} - \frac{\partial}{\partial y}F_{q_y} &= 0 \\ F_Z - \frac{\partial}{\partial x}F_{Z_x} - \frac{\partial}{\partial y}F_{Z_y} &= 0 \end{cases} \tag{16}$$

From (15), approximating the reflectance map around $(p, q)$ by Taylor series expansion of up to first order terms, after some algebraic manipulations we obtain:

$$\begin{pmatrix} \mathcal{R}_p^2 + \mu & 5\mathcal{R}_p\mathcal{R}_q & \mu \\ 5\mathcal{R}_p\mathcal{R}_q & 5\mathcal{R}_q^2 + \mu & \mu \\ -1 & -1 & 4 \end{pmatrix} \begin{pmatrix} \delta p \\ \delta q \\ \delta Z \end{pmatrix} = \begin{pmatrix} C_1 \\ C_2 \\ C_3 \end{pmatrix} \tag{17}$$

where

$$\begin{aligned} C_1 &= (-\mathcal{R} + I + \mathcal{R}_p p_{xx} + \mathcal{R}_q q_{xx} - I_{xx} + \\ &\quad \mathcal{R}_p p_{yy} + \mathcal{R}_q q_{yy} - I_{yy})\mathcal{R}_p - \mu(p - Z_x) \\ C_2 &= (-\mathcal{R} + I + \mathcal{R}_p p_{xx} + \mathcal{R}_q q_{xx} - I_{xx} + \\ &\quad \mathcal{R}_p p_{yy} + \mathcal{R}_q q_{yy} - I_{yy})\mathcal{R}_q - \mu(q - Z_y) \\ C_3 &= -p_x + Z_{xx} - q_y + Z_{yy} \end{aligned}$$

and $(\delta p, \delta q, \delta Z)$ are the increments in $(p, q, Z)$ after an iteration. Solving (17) we obtain the updating scheme

$$\begin{cases} \delta p &= \frac{4}{\Delta}\left[(C_1 - \frac{1}{4}\mu C_3)(5\mathcal{R}_q^2 + \frac{5}{4}\mu) \right. \\ &\quad \left. -(C_2 - \frac{1}{4}\mu C_3)(5\mathcal{R}_p\mathcal{R}_q + \frac{1}{4}\mu)\right] \\ \delta q &= \frac{4}{\Delta}\left[(C_2 - \frac{1}{4}\mu C_3)(5\mathcal{R}_p^2 + \frac{5}{4}\mu) \right. \\ &\quad \left. -(C_1 - \frac{1}{4}\mu C_3)(5\mathcal{R}_p\mathcal{R}_q + \frac{1}{4}\mu)\right] \\ \delta Z &= (C_3 + \delta p + \delta q)/4 \end{cases}$$

where $\Delta$ is the determinant of the coefficient matrix, which is always positive as shown below

$$\begin{aligned} \Delta &= 4\left[(5\mathcal{R}_p^2 + \tfrac{5}{4}\mu)(5\mathcal{R}_q^2 + \tfrac{5}{4}\mu) - (5\mathcal{R}_p\mathcal{R}_q + \tfrac{1}{4}\mu)^2\right] \\ &= 4\left\{5\mu\left[\mathcal{R}_p^2 + \mathcal{R}_q^2 + \tfrac{1}{4}(\mathcal{R}_p - \mathcal{R}_q)^2\right] + 1.5\mu^2\right\} \\ &> 0 \end{aligned}$$

So the iterative scheme is stable.

### 3.2 Implementation

A hierarchical implementation of the SFS algorithm is given below:

**Step 1:** Estimation of the reflectance map parameters $(\tau, \gamma, \eta, \sigma_0)$.

**Step 2:** Normalization of the input image:

$$\hat{I} = (I - \sigma_0)/\eta.$$

Reducing the input image size to that of the lowest resolution layer, and setting the values of $p^o$, $q^o$, and $z^o$ to zeros.

**Step 3:** Updating the current shape reconstruction.

$$\begin{cases} \delta p &= (C_1 A_{22} - C_2 A_{12})/\Delta \\ \delta q &= (C_2 A_{11} - C_1 A_{12})/\Delta \\ \delta Z &= (C_3 + \delta p + \delta q)/4 \end{cases}$$

where

$$\begin{aligned} A_{11} &= 5\mathcal{R}_p^2 + 1.25\mu \\ A_{12} &= 5\mathcal{R}_p\mathcal{R}_q + 0.25\mu \\ A_{22} &= 5\mathcal{R}_q^2 + 1.25\mu \\ C_3 &= -p_x - q_y + Z_{xx} + Z_{yy} \\ C_1 &= (\varepsilon - \epsilon)\mathcal{R}_p - \mu(p^k - Z_x) - 0.25\mu C_3 \\ C_2 &= (\varepsilon - \epsilon)\mathcal{R}_q - \mu(q^k - Z_y) - 0.25\mu C_3 \\ \mathcal{R} &= \mathcal{R}(p^k(x,y), q^k(x,y)) \\ \mathcal{R}_p &= \mathcal{R}_p(p^k(x,y), q^k(x,y)) \\ \mathcal{R}_q &= \mathcal{R}_q(p^k(x,y), q^k(x,y)) \\ \epsilon &= \mathcal{R} - \hat{I}_{(x,y)} \\ \varepsilon &= \mathcal{R}_p(p_{xx} + p_{yy}) + \mathcal{R}_q(q_{xx} + q_{yy}) - \hat{I}_{xx} - \hat{I}_{yy} \\ \Delta &= A_{11}A_{22} - A_{12}^2 \end{aligned}$$

If {(Solution is stable) OR (Iteration has reached $N_{max}$ of current layer)} continue to Step 4, otherwise repeat Step 3.

**Step 4:** If {Current image is in the highest resolution} stop; Otherwise {Interpolate current layer results to higher resolution image domain and go to Step 3}.

## 4 Experimental Results

To illustrate the usefulness of our reflectance map parameter estimator, we first tested the algorithm on a number of synthetic image sets. The synthetic images tested include: (1) spheres, (2) ellipses with the ratio of major axis (parallel to x-axis) to minor axis equals 2, (3) spheres with additive Gaussian noise, and (4) Mozart statue images synthesized from laser range data[1]. For each case, the test images were generated using $\eta = 200$, $\sigma_0 = 0$, and various combinations

[1] The original laser range data was provided by Andres Huertas of the Institute for Robotics and Intelligent Systems, University of Southern California.

of $\tau$ and $\gamma$. For comparison purposes, Pentland's [3] method as well as Lee and Rosenfeld's method [5] were implemented and tested on the same sets of synthetic images. The main conclusions we reached based on the simulations are as follows: compared to other methods, the $\tau$ estimated by our method is more accurate for ellipse and Mozart images, is more robust to noise and boundary disturbance. Our $\gamma$ and $\eta$ estimates are more accurate for Mozart images and when the true $\gamma$ is relatively large. For the synthetic images tested, our method is stable and gives reasonably good results for all the situations considered. The estimates are sufficiently good for applications to SFS. Details of testing results and comparisons are presented in [10].

We next tested the above estimators on some real images. The results are listed in Table 1, in which extensions ".r", ".g", ".b", and ".w" stand for red, green, blue and black/white respectively. We found that the $\tau$ and $\gamma$ estimated by our method are the best in terms of consistency between the results obtained from different color bands of the same image, images of different resolutions, subimages of a large scene, and stereo image pair. In the results given in Table 1, we detect the intensity bias $\sigma_0$ by finding the minimum of the image intensity array and adjust the image intensities by subtracting this bias. Since for most images there are shadow pixels which have the value of the bias, this simple method works quite well.

Figures 1 and 2 show examples of SFS on real images. In these experiments we let $\mu = 1$ and $N_{max}$ for the highest resolution layer to be 500. We observed that better results are consistently obtained for higher values of $\mu$ and $N_{max}$. The partial derivatives of the reflectance map, $\mathcal{R}_p$ and $\mathcal{R}_q$, are computed numerically.

Figure 1(a) shows an input face image. The reflectance map parameters estimated by our algorithm are: ($\tau = 7.74°$, $\gamma = 59.52°$, $\eta = 192.01$, $\sigma_0 = 3$). Figure 1(b) is the height map obtained by the SFS algorithm. Figure 1(c) shows a 3-D plot of 1(b).

Figure 2(a) shows an input pepper image. The reflectance map parameters estimated by our algorithm are: ($\tau = 15.92°$, $\gamma = 58.20°$, $\eta = 255.96$, $\sigma_0 = 0$). Figure 2(b) is the height map obtained by the SFS algorithm. Figure 2(c) shows a 3-D plot of 2(b).

We tested our SFS algorithm on more than ten real images, and examined the SFS results using different illuminant directions. Due to space limitation, only two examples are presented here and the comparison on images generated from the SFS results using different illuminant directions are omitted. Extensive real image results are given in [10].

# 5 Summary

A practical solution to shape from shading (SFS) should include estimation of illuminant direction, surface albedo and reconstruction of shape using the estimated reflectance map parameters. In this paper we presented methods for estimating reflectance map parameters in a Lambertian imaging model. Tests on both synthetic and real images show that our estimators are more robust and accurate than existing methods. We also introduce a new SFS procedure which implements the smoothness assumption by enforcing the gradients of the reconstructed intensity to be close to the gradients of the input image. Under this formulation, the commonly used quadratic smoothness terms are removed and the slope and height maps are updated simultaneously. A hierarchical implementation of the SFS algorithm is presented. Encouraging results using real images are also presented.

# References


[1] B. K. P. Horn and M. J. Brooks, *Shape From Shading*, The MIT Press, Cambridge, Massachusetts, 1989.

[2] B. K. P. Horn, *Robot Vision*, The MIT Press, Cambridge, Massachusetts, 1986.

[3] A. P. Pentland, "Finding the Illuminant Direction", *J. of Optical Society of America: A*, vol. 72(4), pp. 448–455, April 1982.

[4] M. J. Brooks and B. K. P. Horn, "Shape and Source from Shading", In *Proc. of Int. Joint Conf. on Artificial Intell.*, pp. 932–936, Los Angeles, August 1985.

[5] C. H. Lee and A. Rosenfeld, "Improved Methods of Estimating Shape from Shading Using Light Source Coordinate System", *Artificial Intelligence*, vol. 26, pp. 125–143, 1985.

[6] A. P. Pentland, "Linear Shape From Shading", *Int. J. of Computer Vision*, vol. 4, pp. 153–162, 1990.

[7] B. K. P. Horn, "Height and Gradient from Shading", *Int. J. of Computer Vision*, vol. 5(1), pp. 584–595, August 1990.

[8] M. Shao, T. Simchony, and R. Chellappa, "New Algorithms for Reconstruction of A 3-D Depth Map from One or More Images", To appear in *CVGIP: Image Understanding*, March 1991.

[9] Q. Zheng and R. Chellappa, "A Robust Algorithm for Inferring Shape from Shading", Technical Report USC-SIPI 159, University of Southern California, Los Angeles, 1990.

[10] Q. Zheng and R. Chellappa, "Estimation of Illuminant direction, Albedo and Shape from Shading", To appear in *IEEE Trans. Pattern Anal. Machine Intell.*, June 1991.

[11] B. K. P. Horn and M.J. Brooks, "The Variational Approach to Shape From Shading", *CVGIP*, vol. 33, pp. 174–208, November 1986.

[12] R. T. Frankot and R. Chellappa, "A Method for Enforcing Integrability in Shape From Shading Algorithms", *IEEE Trans. Pattern Anal. Machine Intell.*, vol. PAMI-10(4), pp. 439–451, July 1988.

Table 1: Illuminant Direction and Albedo Estimation for Real Images

| Image | Our method | | | | Pentland's method | | Lee & Rosenfeld's method† | | | | |
|---|---|---|---|---|---|---|---|---|---|---|---|
| | $\tau$ | $\gamma$ | $\eta$ | $\sigma_0$ | $\tau$ | $\gamma$ | $\tau$ | $\gamma_o$ | $\eta_o$ | $\gamma_m$ | $\eta_m$ |
| Lenna-1.b | 10.79 | 54.08 | 127.73 | 41.00 | 48.96 | 0.71 | 49.64 | 79.01 | 134.14 | 38.36 | 116.02 |
| Lenna-1.g | 7.74 | 59.52 | 192.01 | 3.00 | 37.98 | 0.96 | 36.86 | 103.36 | 231.25 | 44.68 | 167.62 |
| Lenna-1.r | 9.29 | 42.89 | 190.47 | 54.00 | 39.62 | 0.94 | 39.30 | 48.05 | 193.78 | 27.01 | 187.20 |
| Lenna-1.w | 11.73 | 52.46 | 162.27 | 37.00 | 41.04 | 0.95 | 40.64 | 73.40 | 167.60 | 36.59 | 149.07 |
| Pepper-1.b | 26.09 | 52.77 | 137.46 | 0.00 | 122.19 | 0.43 | 119.09 | 77.02 | 144.03 | 37.74 | 125.87 |
| Pepper-1.g | 32.74 | 45.25 | 221.72 | 0.00 | 151.21 | 0.91 | 151.24 | 56.38 | 226.76 | 30.47 | 214.68 |
| Pepper-1.r | 45.16 | 7.65 | 146.72 | 6.00 | 122.05 | 1.39 | 120.20 | 0.00 | 169.89 | 0.00 | 169.89 |
| Pepper-1.w | 32.04 | 32.27 | 154.23 | 2.00 | 132.39 | 1.05 | 130.71 | 26.83 | 161.68 | 16.69 | 160.65 |
| Pepper-2.b | 21.34 | 56.19 | 172.88 | 0.00 | 76.05 | 2.92 | 79.22 | 87.80 | 188.74 | 40.88 | 154.89 |
| Pepper-2.g | 13.00 | 46.95 | 243.97 | 0.00 | 299.79 | 3.34 | 292.05 | 59.77 | 248.87 | 31.78 | 233.27 |
| Pepper-2.r | 22.56 | 6.50 | 201.31 | 0.00 | 206.88 | 2.66 | 215.91 | 0.00 | 232.87 | 0.00 | 232.87 |
| Pepper-2.w | 20.40 | 24.06 | 173.24 | 0.00 | 282.54 | 0.79 | 277.52 | 0.00 | 186.66 | 0.00 | 186.66 |
| Pepper-3.b | 23.25 | 59.06 | 149.29 | 0.00 | 39.06 | 1.63 | 47.02 | 101.77 | 178.47 | 44.33 | 131.28 |
| Pepper-3.g | 15.92 | 58.20 | 255.96 | 0.00 | 312.61 | 2.05 | 303.75 | 97.25 | 294.16 | 43.29 | 225.05 |
| Pepper-3.r | 22.00 | 17.85 | 185.45 | 11.00 | 304.46 | 0.74 | 297.63 | 0.00 | 207.31 | 0.00 | 207.31 |
| Pepper-3.w | 18.56 | 34.55 | 163.15 | 4.00 | 335.30 | 1.37 | 327.56 | 29.97 | 169.62 | 18.36 | 168.13 |
| Renault-2 | 157.05 | 46.08 | 132.09 | 14.00 | 105.05 | 2.27 | 104.19 | 55.17 | 133.51 | 29.98 | 126.82 |
| Renault-3 | 168.41 | 44.75 | 130.58 | 14.00 | 110.06 | 1.87 | 109.76 | 51.98 | 132.02 | 28.68 | 126.43 |

†$\gamma_o$ and $\eta_o$ indicate the estimates obtained by applying the original form of Lee & Rosenfeld's method. $\gamma_m$ and $\eta_m$ represente the eatimates obtained by applying the shadow compensated Lee & Rosenfeld's method [10].

(a) (b) (c)

Figure 1: SFS result on a face image. (a) The input image. The reflectance map parameters estimated by our algorithm are: $\tau = 7.74°$, $\gamma = 59.52°$, $\eta = 192.01$, and $\sigma_0 = 3$. (b) The height map obtained by the SFS algorithm. (c) A 3–D plot of (b).

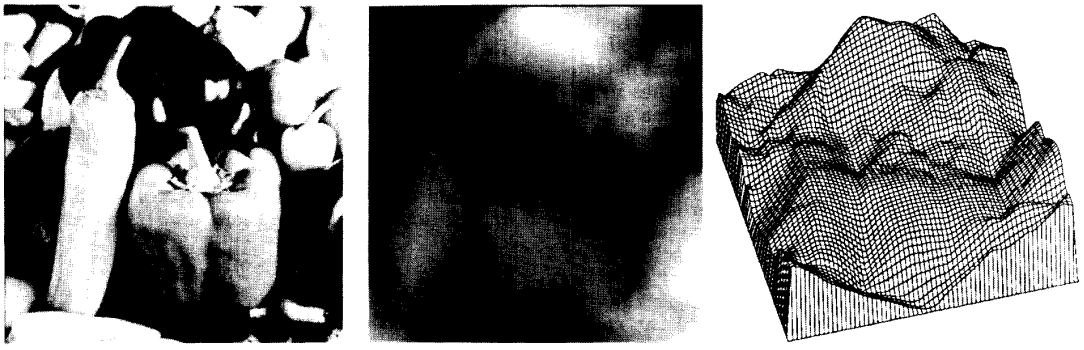

(a) (b) (c)

Figure 2: SFS result on a pepper image. (a) The input image. The reflectance map parameters estimated by our algorithm are: $\tau = 15.92°$, $\gamma = 58.20°$, $\eta = 255.96$, and $\sigma_0 = 0$. (b) The height map obtained by the SFS algorithm. (c) A 3–D plot of (b).